BUTTERWORTH HEINEMANN

Mathematical modeling of brush seals

J. W. Chew and B. L. Lapworth
Aerothermal Methods, Rolls-Royce PLC, Derby, UK

P. J. Millener
Combustion Technology, Rolls-Royce PLC, Bristol, UK

A computational fluid dynamics (CFD)-based model of brush seals has been developed and tested against other workers' experimental data. In the model, the brush is treated as an axisymmetric, anisotropic porous region with nonlinear resistance coefficients. The resistance coefficients are chosen through calibration against measurements. The CFD model gives predictions of flow rate, pressure distribution, velocity field, and bending forces on the bristles. The bristle forces are used in a separate calculation to estimate bristle bending and reaction forces on the shaft and backing plate. Bending in both the axial direction and the orthogonal plane are considered.

Keywords: anisotropic porous media; aerodynamic forces; bristle bending; contact forces

Introduction

Brush seals offer significant benefits over conventional labyrinth seals in gas turbine engines and are currently the subject of considerable research and development work. Despite much experimentation and the fact that brush seals have successfully operated in jet engines (Ferguson 1988) their behavior is far from fully understood. In this paper, a mathematical model is proposed that, it is believed, will reproduce many characteristics of actual brush seals. The model is useful in aiding understanding and in considering the effect of design or operating condition changes.

A schematic of a brush seal is shown in Figure 1. It comprises a pack of wire bristles of diameter 0.076 mm clamped between a front plate (on the high-pressure side) and a backing ring. The bristles are inclined in the orthogonal (r–θ) plane at a lay angle ϕ (typically 45°) to the shaft tangent. Design variables include bristle and backing ring dimensions, bristle material, pack thickness, lay angle, bristle packing (as influenced by method of manufacture), and degree of interference or clearance fit. Important characteristics of the seal include leakage flow rates, pressure-bearing capacity, service life, and tolerance to relative movement of the rotor and stator during operation. Published experimental evidence suggests that this is a complex problem involving coupling of aerodynamic forces, bristle bending, and contact forces. The paper by Chupp and Holle (1994) is recommended to readers for a bibliography of published work on brush seals.

Publications on mathematical modeling of brush seals have focused mainly on aerodynamic effects and fall into two categories; full computational fluid dynamics (CFD) calculations of flow through the pack; or porosity models in which a resistance law is assumed for the "average flow" through the pack. An example of the full CFD approach is given by Braun and Kudriavtsev (1995). Two-dimensional (2-D), laminar, incompressible conditions are assumed, and the flow in the cross section through an array of fixed circular pins is calculated. Some qualitative agreement with flow visualization on a large-scale experimental model is shown. Pressure differences across the array show discrepancies of order 20% between calculation and measurement.

An example of the porosity-type approach is given by Dowler et al. (1992). This is an essentially one-dimensional (1-D) treatment with the flow resistance estimated from work on cylindrical bodies in cross flow. Some encouraging correlations of seal flow data are achieved. In a similar spirit, but differing considerably in detail, Hendricks et al. (1991) have developed a bulk flow model based on results for porous media and filters. These workers also estimated bristle bending by applying standard cantilever beam theory to an isolated single bristle. This is representative of published work on bristle bending to date.

Bayley and Long (1993) have presented an axisymmetric, 2-D model (which they attribute to unpublished work by Owen). Although not entirely clear from the paper, this model is equivalent to treating the brush as an anisotropic, Darcian, porous medium. The authors' "porosity value" is the ratio of resistance coefficients in orthogonal directions. To match pressure measurements on the backing plate, this parameter was typically given a value of 30, indicating considerable anisotropy. This is an important result; although, given the nature of the bristle pack, it may not be surprising.

In the model proposed here, the brush is treated as an anisotropic, porous medium with nonlinear resistance coefficients. The equations are solved using conventional CFD techniques with the porous region embedded in the solution domain. This enables interaction with flow upstream and downstream of the pack to be captured. Aerodynamic forces from this calculation are used in a bending model that includes interaction between rows of bristles.

Fluid dynamics model

The CFD code used here is based on the algorithm described by Moore (1985) and has been applied to many turbomachinery flows (see, for example, Northall et al. 1987). In this code, the

Address reprint requests to Dr. J. W. Chew, Aerospace Group, Rolls-Royce PLC, P. O. Box 31, Derby DE 24 8BJ, UK.

Received 12 January 1995; accepted 12 July 1995

Int. J. Heat and Fluid Flow 16: 493–500, 1995

655 Avenue of the Americas, New York, NY 10010

0142-727X/95/$10.00
SSDI 0142-727X(95)00061-T

governing equations are discretised by integration over a set of control volumes using linear interpolation rules. The discretised equations are iterated toward convergence using the SIMPLER algorithm as described by Patankar (1980).

In flow regions outside the brush, the Reynolds-averaged Navier–Stokes equations with a turbulence model are assumed, as is usual in aerodynamic codes. These equations express conservation of mass and momentum and may be written as follows:

$$\nabla \cdot (\rho \mathbf{u}) = 0 \tag{1}$$

$$\rho \mathbf{u} \cdot \nabla \mathbf{u} = \nabla \cdot \mu_e \nabla \mathbf{u} + \nabla \cdot \mu_e \nabla \mathbf{u}^T - \nabla p \tag{2}$$

where compressibility effects in the viscous terms are taken to be negligible. In these equations ρ, μ_e, p, and $\mathbf{u}$ denote fluid density, effective viscosity, pressure, and velocity vector, respectively. Here the equation for conservation of energy is approximated by a uniform stagnation temperature condition. Note that for adiabatic surfaces and a nonrotating shaft (as is considered below), the bulk stagnation temperature of the air will remain constant, because there is no work or heat input to the system. Variations in stagnation temperature will occur within shear layers in the fluid, but, from comparison with established boundary layer theory (e.g., Schlichting 1979), these are expected to be reasonably small for the conditions considered and are neglected in the present model.

The perfect gas law and a mixing length model of turbulence are also assumed. Boundary-layer thicknesses needed for the mixing length calculations are obtained using a vorticity-based test function. In the outer part of the boundary layer, the mixing length is set to 0.08 times the boundary-layer thickness. In the inner region of the boundary layer, the mixing length is first set to 0.41 times the distance from the wall and then multiplied by a van Driest damping factor.

To model the brush extra source terms (or body forces), representing the drag exerted on the fluid by the bristles, are included in the momentum conservation equations. For the assumed anisotropic, nonlinear resistance law we have the following:

Resistance force per unit volume:

$$\mathbf{F}_r = -\tilde{A}\mu\mathbf{u} - \tilde{B}\rho\,|\mathbf{u}|\,\mathbf{u} \tag{3}$$

where $\tilde{A}$ and $\tilde{B}$ are the viscous and inertial resistance tensors.

For the flow within the brush, the model equations are given by Equations 1 and 2 with the extra resistance forces from Equation 3 added to the right-hand side of the momentum conservation Equation 2. In the study of porous media, it is quite usual to neglect the inertial terms on the left-hand side and the viscous shear stress terms on the right-hand side of Equation 2, leaving a balance between the pressure gradient and porous resistance terms. These terms have not been neglected here, to retain a more complete model (and for convenience of programming). Note, however, that with the present choice of effective viscosity in the brush region, the shear stress terms are not properly modeled. Simple order-of-magnitude estimates indicate that the viscous terms will have little effect in this application.

Consider now the linear resistance term involving the tensor $\tilde{A}$. (For an isotropic, Darcian medium, this would be a diagonal tensor with equal elements, and the nonlinear resistance term would be zero.) We expect $\tilde{A}$ to be symmetric with principal axes in the directions normal to the bristles in the r–θ plane, parallel to the bristles and parallel to the axial direction. Note that a pressure gradient aligned with any of the principal axes will produce motion in that direction only. In general, in an anisotropic porous medium, the velocity may not be in the direction of the pressure gradient. Defining a_n, a_s, and a_z to be resistance coefficients in the principal directions, the elements of $\tilde{A}$ (denoted a_{ij}) have the following form in the natural cylindrical coordinate system for the problem (r, θ, z).

Notation

$a_{i,j}$	viscous resistance tensor components
a_n, a_s, a_z	principal viscous resistance coefficients, normal to bristles in r–θ plane, parallel to bristles, and in axial direction, respectively
$\tilde{A}$	viscous resistance tensor
$A_{i,j}$	bending coefficients, Equation 10
$b_{i,j}$	inertial resistance tensor components
b_n, b_s, b_z	principal inertial resistance coefficients, normal to bristles in r–θ plane, parallel to bristles, and in axial direction, respectively
$\tilde{B}$	inertial resistance tensor
E	modulus of elasticity
F_i	point force on bristle
$\mathbf{F}_r$	resistance force per unit volume
$H_{j,i}$	reaction forces from upstream bristle row
I	moment of inertia
l	bristle length
M	bending moment
p	static pressure
p_d	downstream pressure
p_u	upstream pressure
P	inclined prop force
r	radial coordinate
R	reaction force from downstream bristle row or radius of beam cross section
R_p	pressure ratio = p_u/p_d
s	maximum fiber stress
S_n	shaft reaction component normal to bristle
S_r	shaft reaction force (in radial direction)
$\mathbf{u}$	velocity vector
W	aerodynamic force
x_i	point on bristle
x	distance along bristle length (from tip)
y	normal bristle deflection
y_k	normal bristle deflection caused by point force at $x = x_k$
z	axial coordinate or normal bristle deflection at tip

Greek

β	angle between bristle and backing ring face
Δl	change in projected length
θ	tangential coordinate
μ	viscosity
ρ	density
ϕ	bristle lay angle

Subscripts

e	effective
j, i	bristle row j, location $x = x_i$
oh	denotes location of backing ring edge
t	turbulent

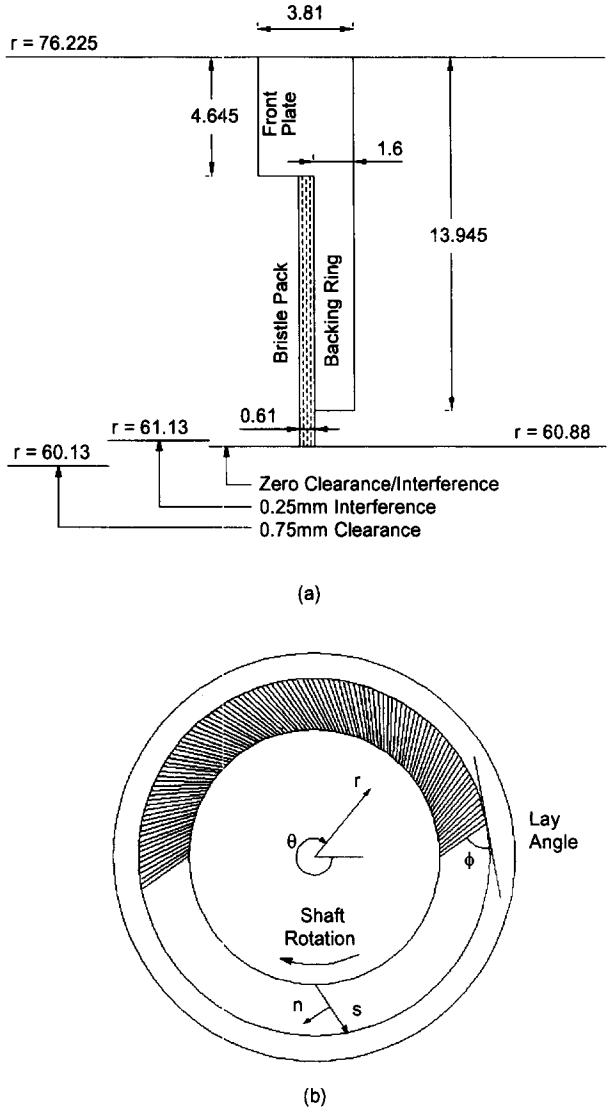

Figure 1 Schematic of brush seal (dimensions in mm)

$$a_{rr} = a_s \sin^2 \phi + a_n \cos^2 \phi, \quad a_{r\theta} = (a_n - a_s) \sin \phi \cos \phi, \quad a_{rz} = 0$$

$$a_{\theta r} = a_{r\theta}, \quad a_{\theta\theta} = a_s \cos^2 \phi + a_n \sin^2 \phi, \quad a_{\theta z} = 0$$

$$a_{zr} = 0, \quad a_{z\theta} = 0, \quad a_{zz} = a_z \tag{4}$$

where the two coordinate systems are defined as shown in Figure 1b. From Equations 3 and 4 it is clear that pack anisotropy leads to coupling of the radial and tangential momentum equations. This coupling underlies the blow-down effect that is be discussed later.

The form of the inertial Term in Equation 3 has been chosen as a simple extension of the well-established resistance law for an isotropic porous medium. It should be noted that alternative formulations of this nonlinear term are admissible and that further work would be required to establish the most appropriate form.

It is assumed that the inertial resistance tensor B has the same form as A. Thus, there are a total of six resistance coefficients a_s, a_n, a_z, b_s, b_n, and b_z to be defined. In the computations here, it is assumed that $a_n = a_z$, $b_n = b_z$, and all coefficients are uniform throughout a bristle pack and do not vary with pressure difference across the seal. The choice of the remaining four constants is described in the Results.

A typical solution domain and calculation mesh is shown in Figure 2. Boundary conditions on solid walls are given by the usual no-slip, no-penetration assumptions. Essentially, at the inlet, total pressure and flow angle are specified, and at the outlet, static pressure is specified. Some special treatment was needed to suppress any flow reversal at inlet and exit during the calculation; this had negligible effect on the results in the region of the seal. Some difficulties were encountered with convergence of the iterative solution in the vicinity of the seal. These were overcome using relaxation and employing a fixed control volume pattern with artificial viscosity to damp oscillations [as opposed to the upwinded control volumes described by Moore (1985)].

Bristle bending model

The aerodynamic force on the bristles is equal in magnitude but opposite in direction to the drag exerted on the fluid by the bristles. Hence, once a converged CFD solution has been achieved, the aerodynamic forces on the bristles may be obtained from Equation 3. The two components of interest for the bending calculations are those in the axial direction, $\mathbf{e}_z \cdot F_r$, and normal to the bristles in the orthogonal plane, $\mathbf{e}_n \cdot F_r$, where $\mathbf{e}$ denotes a unit vector in the direction of the subscript. Noting that in the cylindrical coordinate system $\mathbf{e}_n = (\cos \phi, \sin \phi, 0)$, these two components of force per unit volume are obtained on the CFD calculation mesh. Using bilinear interpolation and a specified bristle-packing density, the forces acting on the bristles are then estimated. The forces will vary along the bristle length and axially through the pack. In this section, we describe how the aerodynamic forces are used to estimate bristle bending.

In this model, first-order bending theory is used, assuming that the bristle deflections are much smaller than the bristle length. This is considered sufficiently accurate for our present purposes and greatly simplifies the problem. To this level of approximation, the axial deflections are independent of the forces and deflections in the r–θ plane. For the bending in the r–θ plane, account is taken only of the axial forces only through the inclined prop effect (which is described later). Frictional and packing effects that introduce further coupling are neglected in the present paper.

The axial and orthogonal plane bending calculations are described separately below. As a precursor to this, some results from standard cantilever beam theory are first given.

Cantilever beam theory

The equation underlying the model is that for the flexion of a straight beam. This can be found in many text books (e.g., Roark 1954) and is written as follows:

$$EI \frac{\mathrm{d}^2 y}{\mathrm{d}x^2} = M \tag{5}$$

where E denotes modulus of elasticity, I is the moment of inertia of the cross section ($= \pi R^4/4$, for a circular cross section beam, radius R), x is distance along the bristle, y is the deflection (normal to the bristle), and M is the bending moment in the plane considered. Here, we take $x = 0$ at the free end of the

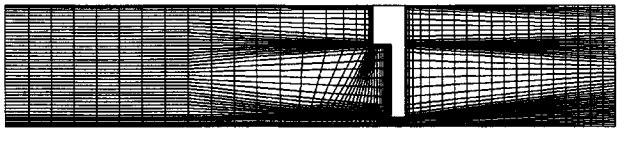

Figure 2 Typical computational mesh

bristle, and at the fixed end $x = 1$, we have the following boundary condition

$$y = \frac{dy}{dx} = 0 \qquad \text{at} \qquad x = 1 \tag{6}$$

In the present problem, aerodynamic forces act along the length of the bristle, and there are contact forces with the backing plate and shaft, and between bristles. The problem may be discretised by defining a number of nodes at locations x_i along the length of the bristle and approximating all the forces on the bristle by point forces F_i at the nodes. The bending moment M is then given by

$$M(x) = \sum_{x_i \leqq x} F_i(x - x_i) \tag{7}$$

From the linear nature of the problem, it follows that we can use the principle of superposition. If $y_k(x)$ is the solution of Equation 5 with boundary condition 6 for a single force F_k acting at $x = x_k$, then $y = \Sigma y_k$ gives the solution of the multiple force problem defined by Equation 7. The compound solution also satisfies boundary condition 6. The solution for y_k is straightforward to derive and is given in standard texts; it may be written as follows:

$$y_k = \begin{cases} \dfrac{F_k}{6EI}\left[(l-x_k)^2(2l+x_k) - 3(l-x_k)^2 x\right] \\ \quad \text{for } 0 \leqq x \leqq x_k \\ \dfrac{F_k}{6EI}\left[x^3 - 3x_k x^2 + 3(2x_k - l)lx + l^2(2l - 3x_k)\right] \\ \quad \text{for } x_k \leqq x \leqq l \end{cases} \tag{8}$$

Using superposition, it may then be deduced that the solution of the problem defined by Equations 5, 6, and 7 at $x = x_i$ is given by the following:

$$y(x = x_i) = \sum_k A_{i,k} F_k / 6EI \tag{9}$$

where

$$A_{i,k} = \begin{cases} \left[(l-x_k)^2(2l+x_k) - 3(l-x_k)^2 x_i\right] \\ \quad \text{if} \qquad x_k \geqq x_i \\ \left[x_i^3 - 3x_k x_i^2 + 3(2x_k - l)lx_i + l^2(2l - 3x_k)\right] \\ \quad \text{if} \qquad x_k < x_i \end{cases} \tag{10}$$

It may be noted that the deflection at $x = x_i$ due to the force at $x = x_k$ is $A_{i,k}F_k/6EI$.

The small deflection theory also gives estimates of the maximum fiber stress s and change in projected length of the beam due to bending Δl. The appropriate formulae are given by Roark (1954) and may be written as follows:

$$s = 4M/\pi R^3 \tag{11}$$

$$\Delta l = \frac{1}{2}\int_0^l \left(\frac{dy}{dx}\right)^2 dx \tag{12}$$

Axial bending calculations

Suppose that the bristle pack consists of m circumferential rows of bristles, the rows being equally spaced in the axial direction, and, in the absence of aerodynamic forces, the bristles in adjacent rows lightly touching. With axial symmetry and n calculation

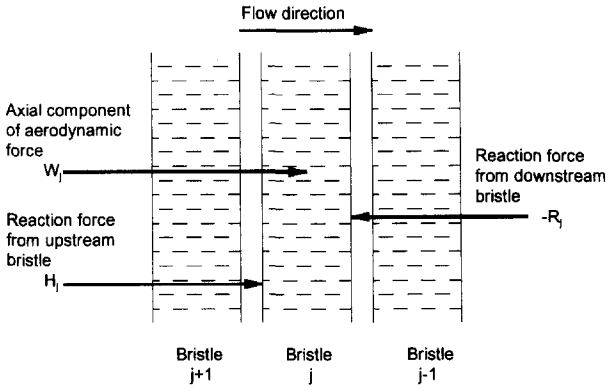

Figure 3 Axial bending forces on bristle j

points along the length of a bristle, the disretized problem reduces to finding deflections and forces at $n \times m$ solution points. If values at the radial position i for a bristle in row j (increasing in the upstream direction from $j = 1$ for the downstream row) are denoted by subscript j, i, the following forces may act at each solution point: $W_{j,i}$, aerodynamic loads at each point; $R_{j,i}$, reaction force from the downstream row (or backing ring if $j = 1$) at location $j - 1$; $H_{j,i}$, reaction force from the upstream row $j + 1$ (if one exists). These forces are illustrated in Figure 3.

The aerodynamic forces are obtained from the CFD solution as outlined above. Reaction forces and deflections ($y_{j,i}$) must be calculated at each point. Frictional forces have been neglected in the axial bending model.

From the condition that when bristles touch there is an equal and opposite reaction force on the two bristles, it is straightforward to relate $H_{j,i}$ to $R_{j+1,i}$ and eliminate H from the problem.

Bristle rows are assumed not to cross, and, where adjacent rows separate, there can be no reaction forces. Hence, the following constraints must be satisfied:

$$\left.\begin{array}{l} R_{j,i} = 0 \qquad \text{if} \qquad y_{j-1,i} > y_{j,i} \\ y_{j-1,i} \geqq y_{j,i} \end{array}\right\} \quad \text{for} \quad 2 \leqq j \leqq m \tag{13}$$

With the backing ring fixed, the downstream row is subject to the following constraints

$$\left.\begin{array}{l} R_{1,i} = 0 \qquad\qquad\qquad\qquad \text{for} \quad i \leqq i_{oh} \\ 0 \geqq y_{1,i} \\ R_{1,i} = 0 \qquad \text{if} \qquad 0 > y_{1,i} \end{array}\right\} \quad \text{for} \quad i > i_{oh} \tag{14}$$

where $1 \leqslant i \leqslant i_{oh}$ gives the portion of the bristle overhanging the backing ring.

Applying the first-order cantilever beam theory to the bristles, Equation 9 gives the following:

$$y_{j,i} = \sum_k A_{i,k}(W_{j,k} + R_{j,k} + H_{j,k})/6EI \tag{15}$$

where the coefficients $A_{i,k}$ are given by Equation 10. Thus, if $H_{j,i}$ is eliminated, as described above, the problem is to find $y_{j,i}$ and $R_{j,i}$, so that Equation 15 with the constraints 13 and 14 are satisfied.

An iterative solution method is used in which an error function is defined at each node, and the reactions are successively adjusted until a specified tolerance is reached. For the examples given later, satisfactory converged solutions were obtained in a few minutes CPU time on on Amdahl 5990-1400.

Bending in the orthogonal plane

For bending in the $r-\theta$ plane, two limiting cases are considered. These assume that either the rows of bristles can move independently without resistance from adjacent rows, or that the bristle pack moves as one, with adjacent rows locked together, as far as normal movements are concerned. We refer to the former case as the frictionless model and the latter case as the bulk model. In the theory and results presented here, no account is taken of friction between the bristle pack and the backing ring edge, although extension to include this is straightforward. Bristle reactions against the shaft are also calculated assuming frictionless contact (although, again, the extension to include a simple frictional model is straightforward).

It is assumed that the bristles can slide freely against each other in their lengthwise direction. Hence, in the bulk model, reactions between the bristles act so as to produce equal bending forces on each bristle, but bristle stiffness is not affected. Averaging the aerodynamic forces over the volume of the bristle pack gives the appropriate forces for the bulk model. Further forces must be considered at the backing ring edge and at the bristle tips when they contact the shaft.

At the backing ring edge, the inclined prop effect gives a force in the $r-\theta$ plane, which tends to close the bristle to shaft clearance. This force arises from the combined effect of the bristle lay angle and the axial deflection of the bristle. Denoting this force by P, we have the following from Rees (1988);

$$P = R \tan \beta / \tan \phi \qquad (16)$$

where R is the axial reaction at the backing ring edge, β is the angle between the bristle and the backing ring face ($= 0$ when there is no axial deflection), and ϕ is the bristle lay angle as usual. In the bulk model, this force is averaged over all the bristles; whereas, in the frictionless model, it is applied only to the downstream bristle row. The inclined prop force will be small relative to the axial forces. However, aerodynamic forces in the $r-\theta$ plane are also smaller than the axial forces, and so the inclined prop effect may be significant for $r-\theta$ plane bending.

If the bristle tip contacts the shaft, then a reaction force on the shaft is generated. This force is obtained from the restriction on shaft deflection at this point. To satisfy this condition, a point force S_n acting normal to the bristle may be required. Because, for frictionless conditions, the shaft reaction S_r must be normal to the shaft surface, we obtain

$$S_r = S_n / \cos \phi \qquad (17)$$

S_r has units of force; to obtain the average pressure on the shaft it is necessary to multiply by the number of bristles per unit area in the $\theta-z$ plane.

Solutions of the bristle-bending equations for the frictionless model are obtained using Equation 9. Compared to the axial bending calculations, the $r-\theta$ plane bending calculations are computationally very quick.

Results

Correlation of the model against Bayley and Long's (1990, 1993) experimental data for the seal shown in Figure 1 (with a 0.25mm interference fit) is described in the subsection Choice of resistance coefficients. Some further predictions from the model are then presented in later subsections.

In the calculations presented in the following subsections, typical CFD meshes used had 76 axial and 48 radial grid locations. The bending calculations used similar step sizes along the length of the bristle to those in the CFD calculation. Eight rows of bristles and a pack thickness of 0.61mm were assumed. Fluid and material properties were chosen to approximately match experimental conditions. Shaft rotation is not included in these calculations or in the experiments to which the data is compared.

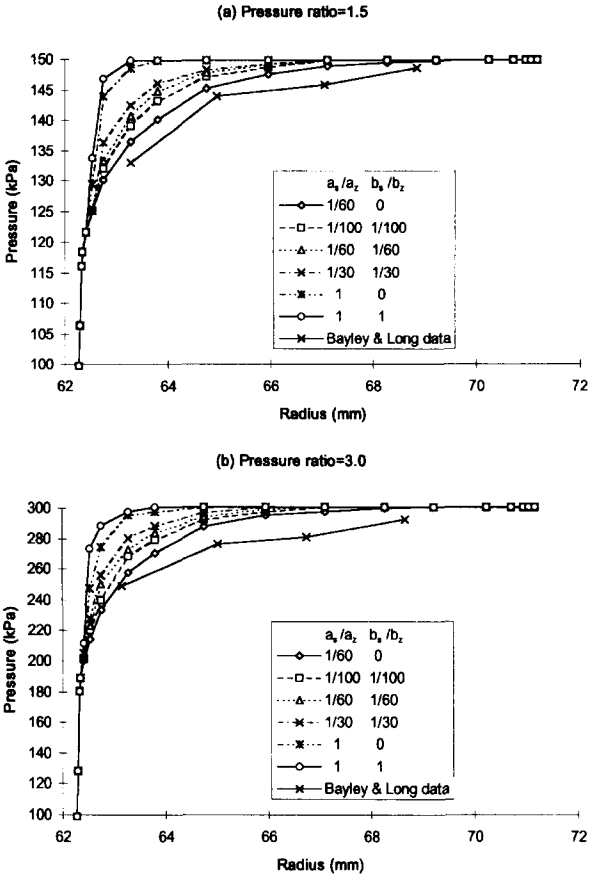

Figure 4 Comparison of calculated and measured backing ring pressures for the 0.25mm interference seal: (a) pressure ratio = 1.5; (b) pressure ratio = 3.0

A mesh dependency test was conducted for one example. For conditions corresponding to the interference seal at a pressure ratio of 3, a solution was obtained on a grid with 85 axial and 79 radial locations. Compared to the standard mesh, this mesh had twice the number of grid locations in both directions within the bristle pack. Some mesh dependency was found. For example, mass flow, pressure exerted by the bristle pack on the shaft (according to the bulk model), and maximum axial bristle deflection were found to differ by 4%, 12%, and 4%, respectively, between the two calculations. Although not insignificant, the level of numerical inaccuracy indicated was considered acceptable for an initial evaluation and demonstration of the model.

Choice of resistance coefficients

As stated above, the four resistance coefficients a_z, b_z, a_s, and b_s must be specified in the CFD calculation. These have been obtained through comparison with Bayley and Long's (1990, 1993) flow rate and backing ring pressure measurements. Mass flow rates are principally controlled by the axial resistances a_z and b_z, while backing ring pressures depend mainly on the degree of anisotropy. This methodology is similar to that adopted by Bayley and Long. In the present notation, Bayley and Long's model corresponds to $b_s = b_n = b_z = 0$, $a_n = a_z$. A typical value of the anisotropy coefficient assumed by Bayley and Long is 30; for the present notation this gives $a_z = 59 a_s$.

The effect of assuming various values of a_s and b_s on the backing ring pressure distribution is illustrated in Figure 4. For all calculations in this figure, $a_z = 5.317 \times 10^{11}$ m^{-2}, and $b_z =$

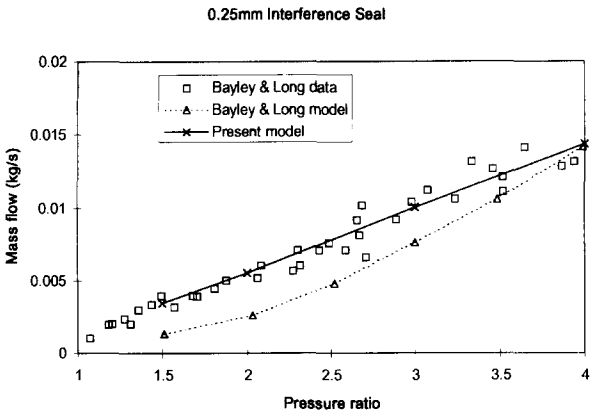

Figure 5 Comparison of calculated and measured mass flow rates

1.998×10^6 m^{-1}. It is clear from this figure that, in order to match the measurements, the porous region must be highly anisotropic. It was found that $a_z = 60a_s$ with $b_s = 0$ gave the best fit to the measurements (of the values tried). Setting $b_s = 0$ implies no inertial resistance in the direction of the bristles and is justified, to some extent, by the relatively straight flow path available in this direction compared to the tortuous path that the gas must follow as it traverses the bristle pack axially. Within the limits of the homogeneous porosity treatment, the level of agreement attained between the model and experimental data is considered reasonable. It may also be noted that the backing ring pressure measurements are subject to some scatter. (The lines joining Bayley and Long's (1990) datapoints are included as visual aids only.)

The calculated and measured mass flow characteristic for this seal is shown in Figure 5. Good agreement is evident for the present model. For the linear (Bayley and Long 1993) model, the agreement is not so good. In the calculations shown in Figure 5, and in all further interference seal predictions described below, the following resistance coefficients have been assumed.

$$a_z = a_n = 60a_s = 5.317 \times 10^{11}\ m^{-2},$$

$$b_z = b_n = 1.998 \times 10^6\ m^{-1}, \qquad b_s = 0$$

It can be noted that, in Figure 5, extrapolation of the present results to $R_p = 1$ might appear to give a nonzero flow rate at this point. Although the numerical studies have not been extended to $R_p < 1.5$, it may be shown from a one-dimensional (1-D) analysis that, with the above values of a_z and b_z, a steepening in gradient of the mass flow–pressure ratio curve is to be expected as R_p approaches unity.

Fluid dynamics

Examples of the predicted velocity field in the vicinity of the seal are given in Figure 6. Consider first Figure 6a, which gives results for the seal in Figure 1 running with 0.75mm clearance, at a pressure ratio of 1.5 and atmospheric conditions downstream. Because the bristle pack is assumed to be undisturbed in these calculations, the resistance coefficients are as for the interference seal above. These vector plots show that the leakage occurs predominantly through the clearance in these circumstances. Flow in the bristle back is relatively weak and is radially inward. Consistent with this flow pattern and experimental observation (Ferguson 1988) aerodynamic forces tend to bend the bristles toward the shaft in this solution. This is sometimes called the blow-down effect.

Figure 6b gives the velocity field for the same conditions as Figure 6a, except that the bristle pack is assumed to be fully blown down. (In this case, the resistance coefficients have been adjusted to give better agreement with experimental leakage rates.) This flow pattern is also representative of interference fit seals. Note the strong 2-D effects and the radially inward flow in front of the backing ring.

Bristle bending

Examples of the bending predictions, from the frictionless model, are shown in Figure 7, for the interference fit seal at pressure ratio $R_p = 4$. Despite the fact that bending forces in the axial direction are considerably larger than those in the r–θ plane, the results show that axial deflections are comparatively small. This is because of the propping effect of the backing ring. The bristles tend to pivot against the backing ring edge and move away from the backing ring face at higher radii. This behavior may lead to high flow resistance in the pack near the backing ring edge, and low resistance in front of the backing plate at higher radii. The measured pressure distributions in Figure 4 appear consistent with this interpretation.

The r–θ plane bristle deflections in Figure 7b indicate that the upstream bristles depart little from the curvature produced by the interference fit. The aerodynamic bending forces become progressively stronger moving downstream through the pack — tending to press the bristle tips against the shaft and produce more bending. For the downstream bristle row, the aerodynamic

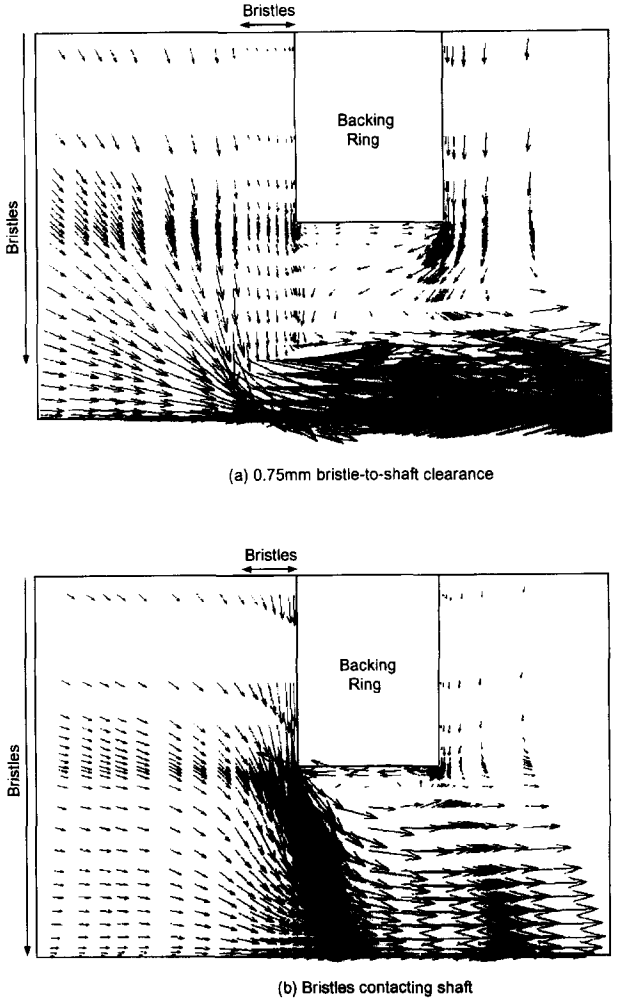

Figure 6 Velocity vectors for 0.75 mm build clearance seal in open and blown-down conditions, pressure ratio = 1.5; (a) 0.75 mm bristle-to-shaft clearance; (b) bristles contacting shaft

and inclined prop forces combine to produce noticeably stronger bending of these bristles.

Further predictions from the bulk-bending model for the interference seal are presented in Figure 8. These results are intended both to illustrate the capability of the model and to summarize the predictions for some important parameters. In the $r-\theta$ plane bending calculations (for estimation of shaft pressure), the bulk bending model was assumed.

Shaft pressures, shown in Figure 8a, will have an important influence on bristle and shaft wear. The figure shows that, for the interference seal, the shaft pressure may rise well above the level caused by the interference fit. This is readily attributed to aerodynamic and inclined prop forces. The inclined prop effect becomes more important (relative to direct aerodynamic forces) at higher pressure differences, and accounts for the nonlinear form of the curve at a pressure difference of 500 kPa. Note that, although an average shaft pressure for the pack has been presented here, significant variations occur between the bristle rows. This is illustrated by the bristle bending curves in Figure 7.

Figure 8b gives maximum axial deflections, which occur at the downstream bristle tips. One point to note from these results is that for the (small) deflections indicated the change in projected length of the bristle given by Equation 12 will also be very small. Hence, the axial bending will not directly lead to significant lift-off of bristles from the shaft for these conditions.

Conclusions

The objective of producing a mathematical model for brush seals has been achieved. Predictions from the model are in agreement with experimental observations, and use of the model has already considerably improved our understanding of brush seal behavior. Compared to other published models, the present model is considered a major advance. There are many interesting aspects of the predictions from the model, and some of these have been presented here.

This study confirms the need for an anisotropic treatment of the bristle pack and shows the (circumferentially averaged) flow in the pack to be highly 2-D. A nonlinear porous resistance law has been shown to give better agreement with measurements than the linear, Darcian treatment. The form of the resistance law used here has been chosen fairly arbitrarily, and the resistance coefficients have been obtained through correlation against limited experimental data. A single set of resistance coefficients was found to give good agreement with mass flow measurements for an interference seal at pressure ratios up to 4. These coefficients did not give agreement with measured mass flow rates for a build clearance seal when it was assumed to be fully blown down. This suggests either a significant change in bristle packing for the blown down seal or incomplete blow down of the seal in the experiment. Clearly, there is scope for further investigations of both the resistance laws assumed and the behavior of build clearance seals.

Calculations of bristle bending have shown that, for the particular seal studied, deflections in the axial direction are quite small. Larger deflections are seen in the orthogonal plane, with the aerodynamic forces tending to press the bristles against the shaft. This confirms the observations of Ferguson (1988).

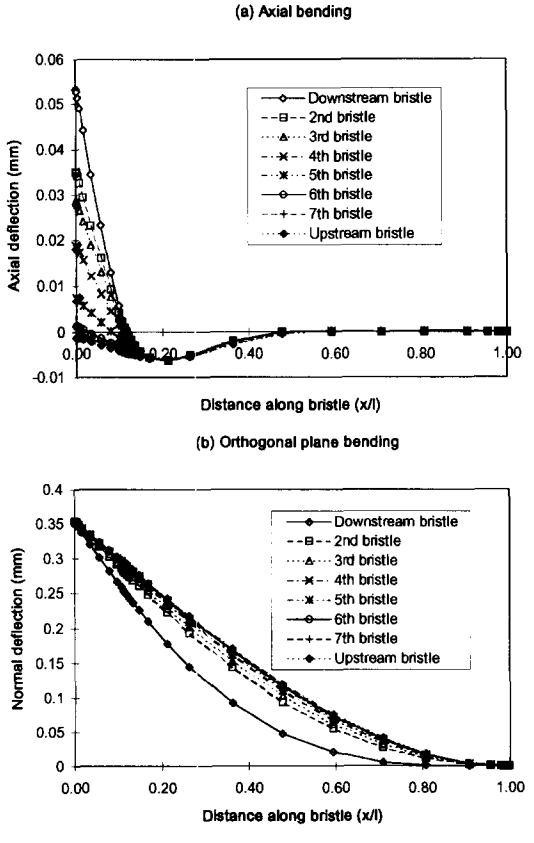

Figure 7 Bending predictions, 0.25 mm interference seal, pressure ratio = 4.0: (a) axial bending; (b) orthogonal plane bending

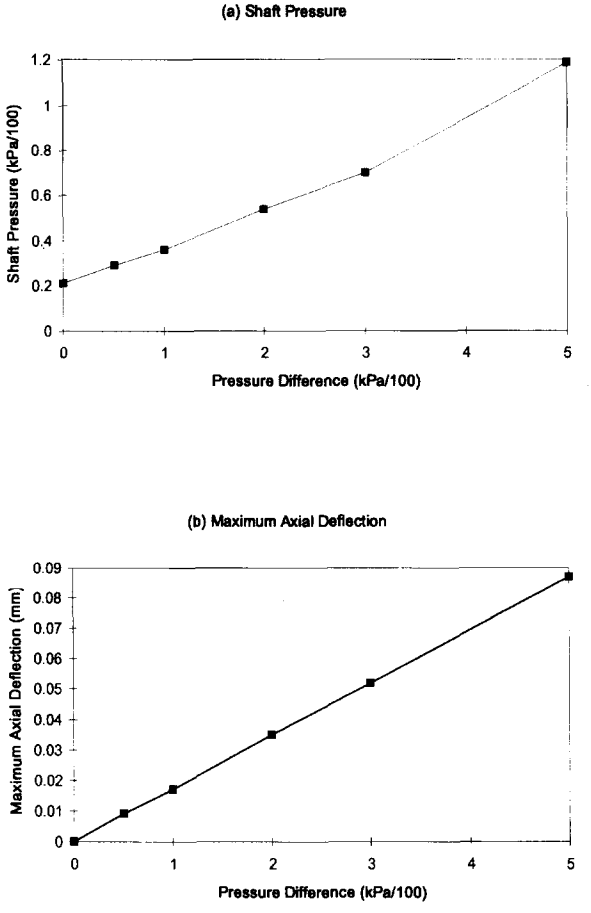

Figure 8 Summary of bending calculations for the 0.25mm, interference seal: (a) shaft pressure; (b) maximum axial deflection

Building on the basic approach presented here, further developments of the model can be expected. For example, coupling of the bending calculation with the CFD solution so that the position of the bristle pack is calculated automatically is feasible. Testing against experimental data, and numerical investigation of different configurations are also clearly of interest and are in progress.

Acknowledgments

We thank our colleagues A. S. Squires M. T. Turner, and P. A Withers for support and helpful technical discussions regarding this work.

References

Bayley, F. J. and Long, C. A. 1990. A theoretical and experimental study of the operation of a brush seal: A final report on non-rotating seals. University of Sussex report 90/TFMRC/122

Bayley, F. J. and Long, C. A. 1993. A combined experimental and theoretical study of flow and pressure distributions in a brush seal. *J. Turbomachinery,* **115**, 404–410

Braun, M.J. and Kudriavtsev, V.V. 1995. A numerical simulation of brish seal section and some experimental results, *J. Turbomachinery*, **117**, 190–202

Chupp, R. E. and Holle, G. G. 1994. Generalizing circular brush seal leakage through a randomly distributed bristle bed. ASME Paper 94-GT-71.

Dowler, C. A., Chupp, R. E. and Holle, G. F. 1992. Simple effective thickness model for circular brush seals. AIAA Paper 92-3192, 28th Joint Propulsion Conference

Ferguson, J. G. 1988. Brushes as high-performance gas turbine seals. ASME Paper 88-GT-182

Hendricks, R. C., Schlumberger, S., Braun, M. J., Choy, F. and Mullen, R. L. 1991. A bulk flow model of a brush seal system. ASME Paper 91-GT-325

Moore, J. G. 1985. Calculation of 3D flow without numerical mixing. AGARD lecture series no. 140 on 3-D computational techniques applied to internal flows in propulsion systems

Northall, J. D., Moore, J. G. and Moore, J. 1987. Three-dimensional viscous flow calculation for loss prediction in turbine blade rows. *Proc. I. Mech. E. Conf. on Turbomachinery — Efficiency prediction and improvement*

Patankar, S. V. 1980. *Numerical Heat Transfer and Fluid Flow*, B. J. Smith et al. (eds.). Hemisphere, Bristol, PA

Rees, B. K. 1988. Brush seal axial load effects on bristle rotor reaction forces. Rolls-Royce Report MCR95013

Roark, R. J. 1954. *Formulas for Stress and Strain*, 3rd ed., McGraw-Hill, New York.

Schlichting, H. 1979. *Boundary-Layer Theory*, 7th ed., McGraw-Hill, New York